Photolysis of solid NH$_3$ and NH$_3$–H$_2$O mixtures at 193 nm

M. J. Loeffler[1,2] and R. A. Baragiola[2,a)]

[1]*Astrochemistry Laboratory, NASA Goddard Space Flight Center, Code 691, Greenbelt, Maryland 20771, USA*
[2]*Laboratory for Atomic and Surface Physics, Engineering Physics, University of Virginia, Charlottesville, Virginia 22904, USA*

We have studied UV photolysis of solid ammonia and ammonia-dihydrate samples at 40 K, using infrared spectroscopy, mass spectrometry, and microgravimetry. We have shown that in the pure NH$_3$ sample, the main species ejected are NH$_3$, H$_2$, and N$_2$, where the hydrogen and nitrogen increase with laser fluence. This increase in N$_2$ ejection with laser fluence explains the increase in mass loss rate detected by a microbalance. In contrast, for the ammonia–water mixture, we see very weak signals of H$_2$ and N$_2$ in the mass spectrometer, consistent with the very small mass loss during the experiment and with a <5% decrease in the NH$_3$ infrared absorption bands spectroscopy after a fluence of ∼3 × 10^{19} photons/cm^2. The results imply that ammonia–ice mixtures in the outer solar system are relatively stable under solar irradiation. © *2010 American Institute of Physics*. [doi:10.1063/1.3506577]

I. INTRODUCTION

The equilibrium phase diagram of the ammonia–water system shows that hydrated H$_2$O:NH$_3$ compounds form in the ratios 1:2 (hemihydrate), 1:1 (monohydrate), and 2:1 (dihydrate).[1] In the solid phase, these different hydrates have distinct crystal structures and infrared absorption spectra.[2,3] These mixtures are almost certainly present in comets[4] and in grains in the atmospheres of the giant planets. Ammonia was also predicted to exist in icy satellites in the outer Solar system.[5,6] Since ammonia lowers the melting point of water drastically, by ∼100 K, it could allow cryo-volcanism in icy satellites around Saturn and Uranus.[7] In fact, an erupting subsurface liquid may be the source of the spectacular polar plumes in the Saturnian moon Enceladus.[8] The presence of ammonia in Enceladus has been discussed, for instance, by Kargel,[9] deduced by Ostro[10] from radar backscattering observations, and used by Stegman[11] to propose a double layer subsurface ocean with water below and ammonia dihydrate on top. The most recent evidence for the presence of ammonia is its detection in Enceladus' plume by Cassini's mass spectrometer.[12]

However, ammonia has only been identified on Charon[13] and possibly a few other icy satellites,[14] through the observation of a very weak absorption feature in their near infrared reflectance spectra. A leading explanation for the discrepancy between expectations and observations is that ammonia is quickly depleted from the surface by energetic ion irradiation[15] with respect to the bulk of the ice, where radiation would not penetrate. This was based on experiments that showed that the sputtering yield of pure solid ammonia under 1.5-MeV He$^+$ bombardment is ∼18 times higher than it is for water ice. Those initial studies on pure ammonia have been recently extended to the more relevant case of ammonia–water mixtures,[3,16–18] which show ion irradiation indeed depletes ammonia preferentially relative to water ice.

While it has been shown in the laboratory that ammonia is efficiently destroyed by ion irradiation, other radiation processes, such as UV photolysis, may also destroy ammonia efficiently. As an example, Lyman-alpha (121.6 nm, 10.2 eV) photons on solid NH$_3$ can produce NH$_2$ and N$_2$H$_4$.[19] We note that while Lyman-alpha radiation can destroy ammonia, it is also strongly absorbed by water ice, the likely host of ammonia on icy surfaces. In this case, ammonia below the surface, but still in the depth range sampled by infrared spectroscopy, will be shielded. Besides Lyman-alpha, higher wavelength UV radiation (<205 nm) is absorbed by solid ammonia[20] and can potentially destroy ammonia. This higher wavelength radiation will penetrate more deeply since it is not absorbed by water, and thus, potentially destroy ammonia over the range observed by remote sensing.

In this study, we investigated the stability of solid NH$_3$ and NH$_3$ mixed in water under the influence of higher wavelength UV irradiation, using a 193 nm ArF excimer laser. Photodesorption photochemistry at this wavelength has been previously studied for NH$_3$ (Ref. 21) and NH$_3$:H$_2$O (1:5) at 90–130 K and for NH$_3$ films at 80 K.[22] In our work, we focus on quantitative photochemistry of the solid using with microbalance gravimetry, mass spectroscopy, and infrared spectroscopy.

II. EXPERIMENTAL SETUP AND METHODS

All experiments were performed in a cryopumped vacuum chamber on a radiation-shielded cryostat (for more details see Ref. 23). The base pressure of the chamber was ∼10^{-10} Torr and 1–2 orders of magnitude better inside the shield. Solid ammonia and ammonia–water films were grown at 40 K by vapor deposition on the optically flat gold mirror electrode of a 6-MHz quartz-crystal microbalance (QCM). The areal mass Q (mass/area) of the films were determined by the change in the resonance frequency of the crystal, which was measured with an Inficon IC/5 controller to a resolution of 0.1 Hz.[24] The measured Q can be converted to film column density η (molecules/cm^2) by dividing by the molecular mass,

a)Author to whom correspondence should be addressed. Electronic mail: raul@virginia.edu.
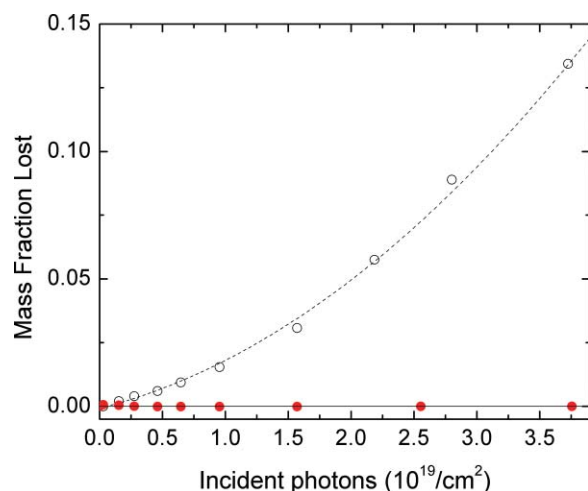
FIG. 1. Cumulative mass loss on the QCM for 660 ML of solid ammonia (○) and a 660 ML ammonia–1300 ML water mixture (●) irradiated at 40 K. The dotted line is a quadratic fit to the data for pure solid ammonia, while the horizontal solid line indicates zero mass lost.

if the film composition is known, and converted to thickness if the mass density is known.

In the experiments reported here, pure NH_3 films contained 6.6×10^{17} molecules/cm^2 or 660 ML (we define a monolayer (ML) as 10^{15} molecules/cm^2). The ammonia–water mixtures contained 660 ML of NH_3 and 1300 ML of H_2O. Mixtures were grown using two separate gas dosers adjusting the relative gas fluxes to achieve the 1:2 NH_3: H_2O ratio of the dihydrate, one of the equilibrium phases for ice mixtures with <65.4 wt% ammonia.[5, 25] In this way, we avoided problems that occur when dosing gaseous mixtures, caused by species-dependent conductance and wall processes in the gas doser.

The films were irradiated at normal incidence with pulses of 193 nm (6.4 eV) light produced by an ArF excimer laser. To ensure uniformity across the sample surface, the laser beam was defocused using an MgF_2 lens ($f = 50$ cm) to cover a rectangular spot ~25 mm × 75 mm at the target, significantly larger than the active diameter of the microbalance (6 mm). To measure the photon flux at our sample, we placed an apertured Ophir power meter at the location of the QCM, which measured constant beam intensity across the area of the QCM. This measurement was used to calibrate those made outside of our vacuum system, enabling us to monitor the output of the laser in real-time during our experiment. The fluence measured at our sample was 1.56×10^{15} photons/cm^2/pulse, which includes the 20% light reflected from the gold substrate.[26] The energy per pulse varied <5% during the experiments and the repetition rate was varied between 0.2 and 5 Hz in different experiments to check for nonlinear effects; however, the majority of experiments were performed at 5 Hz. We note that the low fluence per pulse ensures negligible nonlinear effects due to heating or multiphoton absorption.

A Dycor M200 quadrupole mass spectrometer (MS) monitored the species ejected (photodesorbed/sputtered) during irradiation. The specular reflectance of the films on the gold mirror was measured in the infrared at an incident angle of 35° using a Thermo-Nicolet Nexus 670 Fourier Transform

infrared spectrometer at 2-cm^{-1} resolution. The spectra were divided by the spectrum of light reflected from the bare gold mirror substrate taken before film deposition. These ratios $R(\lambda)$ were then converted to optical depth units, $-\ln[R(\lambda)]$. The areas of the absorption band were derived from $-\ln[R(\lambda)]$ after subtraction of baselines that matched the continuum at both sides of the bands.

III. RESULTS

Figure 1 shows the mass loss through photodesorption, measured by the QCM as a function of laser fluence, for pure NH_3 and ammonia–water samples irradiated at 40 K. For the pure NH_3 sample, we find that there was significant desorption: after 3.7×10^{19} photons/cm^2 the sample has lost ~100 ML (14% of the total mass). The mass loss increases first linearly with fluence; the slope gives a desorption yield of 1.1×10^{-3} per photon, taking the mass loss as mostly due to ejected NH_3.[21, 22] At higher fluences, desorption is dominated by a quadratic component, hinting at changes in the sample composition. We also tested for nonlinear effects by varying the flux on the sample by over a factor of two and found none (data not shown here). Interestingly, irradiation of the same amount of ammonia in a mixture of 1:2 with water ice produces, after the same laser fluence, a mass loss that is ~200 times lower than that measured for the pure ammonia sample.

Figure 2 shows the sputtered flux coming from our NH_3 sample as measured by our mass spectrometer. Of the masses monitored: 2, 13, 14, 15, 17, 18, and 28–32 amu, the most pronounced signals are for 2, 14, 17, and 28, and weaker signals for 15 and 18 amu. The main signals are due to H_2, N (likely from cracking of N_2 or NH_3), NH_3, and N_2, while the weaker signals are assigned to NH, NH_4 or contaminant H_2O. We note that the ratio between the intensity of the 14 and 28 amu
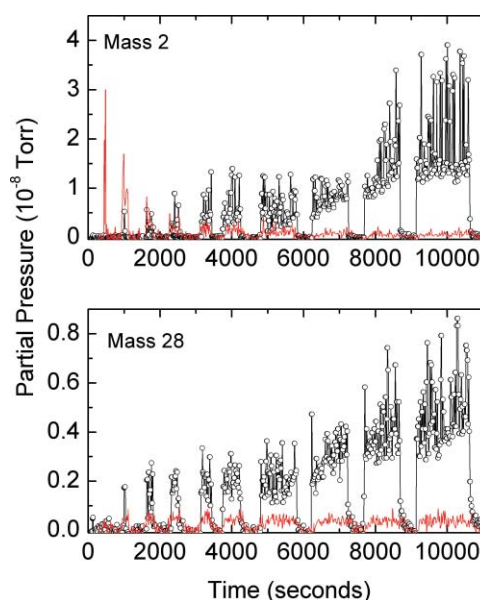

FIG. 2. H_2 and N_2 ejection during irradiation of pure NH_3 film (−○−) and NH_3–H_2O mixture (----) at 40 K, with the beam being pulsed on and off. During one second, the film receives 7.8×10^{15} photons/cm^2. The film composition was 660 ML (pure NH_3) and 660 ± 100 ML of NH_3 and 1350 ± 100 ML of H_2O for the mixture.
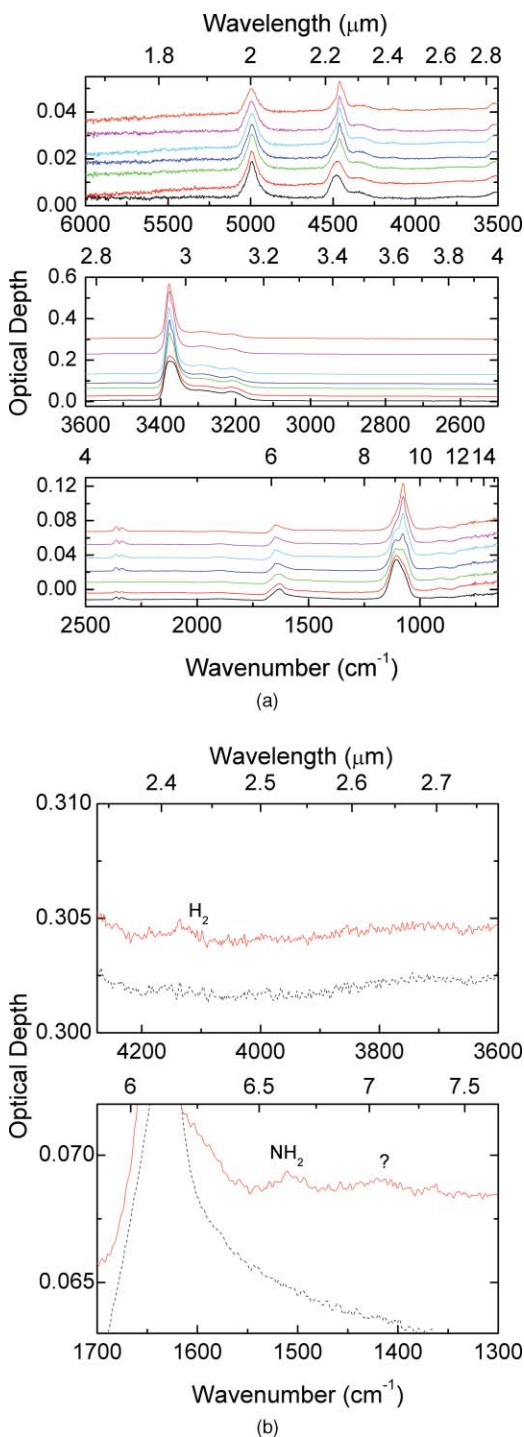
FIG. 3. (a) IR spectra of a 660 ML solid NH$_3$ sample during irradiation. The spectra have been vertically offset for clarity. Spectra from bottom to top in all panels are for 0, 0.031, 0.15, 0.46, 0.95, 2.2, and 3.7×10^{19} photons/cm^2. (b) IR spectra of a 660 ML solid NH$_3$ sample during irradiation. The bottom curve (dashed line) in each panel is the spectrum before irradiation and the upper one (solid line) is after a fluence of 3.7×10^{19} photons cm^{-2}. The structure labeled with a question mark has not been identified.

FIG. 4. IR spectra of bending region of a 660 ML NH$_3$ sample before (1) and after irradiation with 3.7×10^{19} photons cm^{-2} (2), and compared with a crystalline sample of ammonia grown at 80 K and cooled to 40 K (3).

nitrogen signal is significantly suppressed, compared to that of pure ammonia, consistent with the results of our microbalance. We note an initial spike in H$_2$ production from the mixture, which is not present in pure ammonia.

Figure 3(a) shows the infrared spectra of solid NH$_3$ during photolysis. We find that some of the infrared absorption features narrow during irradiation, which is typically attributed to an increase in order in the sample, as exemplified by the sharper bands from a crystalline sample grown at 80 K and cooled to 40 K for irradiation (Fig. 4). A possible explanation is that the sample crystallizes due to the local heating around the molecule that absorbs the photon [we discard macroscopic heating due to the low power of the laser, 1.5 mJ/cm^2 (Ref. 27)]. We note, however, that no absorption bands of the irradiated sample can be reproduced simply by a combination of spectra of crystalline and amorphous ammonia.

Figure 3(b) shows that irradiation produces a very weak band for H$_2$ at 4130 cm^{-1}, one at 1508 cm^{-1}, and an unidentified band at $\sim$1420 cm^{-1}. There is no discernable N$_2$ band at 2325 cm^{-1}, unlike our previous experiments using 100 keV proton irradiation, where it was detected but much weaker than the H$_2$ band.[16]

Figure 5(a) shows the infrared spectra of the ammonia–water mixture during photolysis. Unlike for the pure ammonia sample, here there is no apparent narrowing of the absorption features with fluence. During photolysis we see the loss of a weak feature at 3706 cm^{-1} [Fig. 5(b)] which is likely a dangling bond. We also see the formation of a weak H$_2$ feature at 4139 cm^{-1} [Fig. 5(b)] appears after very high laser pulses and an absorption band at 1496 cm^{-1}, with a 43 cm^{-1} FWHM, which is probably due to NH$_2$ (see below).

IV. DISCUSSION

A. Radiation pathways

Photon absorption of the pyramidal ground state of NH$_3$ at 193 nm leads to two primary, spin-allowed,

signals is $\sim$0.15, which is consistent with the observed cracking pattern of N$_2$ in the mass spectrometer. In contrast, the sputtered flux coming from our ammonia–water sample contained mainly H$_2$ and N$_2$, an order of magnitude smaller signal due to O$_2$ and possibly a weak mass 18 signal which cannot be identified with certainty above background. The
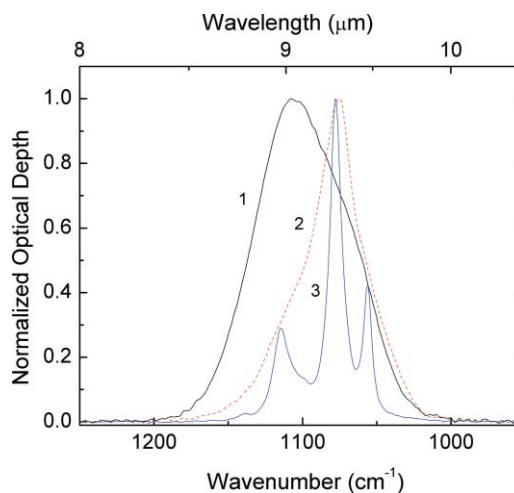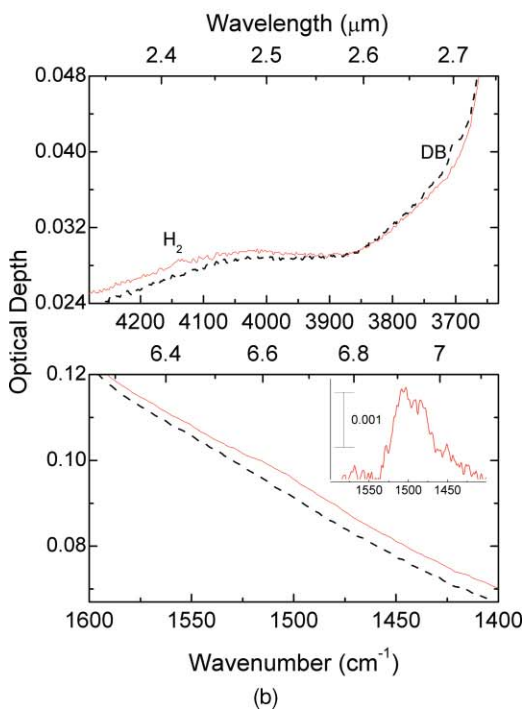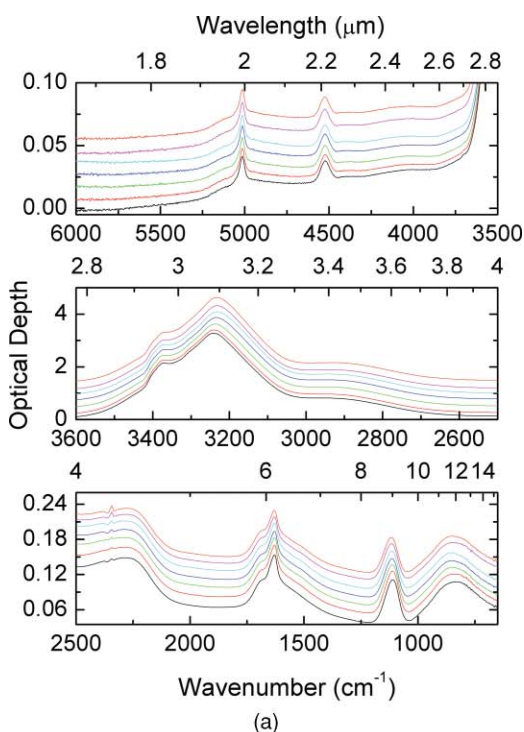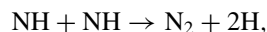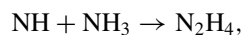
FIG. 5. (a) IR spectra of 660 ML NH_3 and 1300 ML H_2O mixture irradiated at 40 K. The spectra have been vertically offset for clarity. Spectra from bottom to top in all panels are for 0, 0.031, 0.15, 0.46, 0.95, 2.6, and 3.7×10^{19} photons/cm^2. (b) IR spectra of new features detected in 660 ML NH_3 and 1300 ML H_2O mixture irradiated at 40 K: before (dashed) and after 3.7×10^{19} photons/cm^2 (solid). The inset in the bottom panel shows the 1500 cm^{-1} band after subtracting the spectra after irradiation by the spectrum before irradiation.

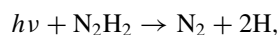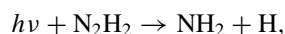photoabsorption processes[28]

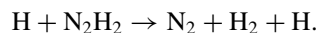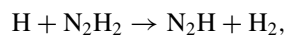$$hv + NH_3 \rightarrow NH_2(\tilde{X}\,^2B_1) + H(> 4.6eV),$$

$$hv + NH_3 \rightarrow NH(a\,^1\Delta) + H^2(> 5.7eV).$$
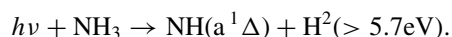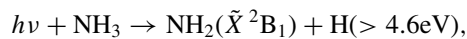
The given threshold energies are for the gas phase, and increase by $\sim$1.3 eV in the solid.[20] NH and NH_2 can be dissociated by subsequent photons to produce N atoms. Besides the back reactions involving H atoms, the main secondary reactions are as follows:

$$NH + NH_3 \rightarrow N_2H_4,$$

$$NH + NH \rightarrow N_2 + 2H,$$

$$NH_2 + NH_2 \rightarrow N_2H_4.$$

The diimide molecule, N_2H_2, is destroyed by photons

$$hv + N_2H_2 \rightarrow NH_2 + H,$$

$$hv + N_2H_2 \rightarrow N_2 + 2H,$$

or by radicals

$$H + N_2H_2 \rightarrow N_2H + H_2,$$

$$H + N_2H_2 \rightarrow N_2 + H_2 + H.$$

It is important to notice that a significant process in thin films is the loss of hydrogen from the solid, analogous to what allows the buildup of oxygen in water ice. Besides ejection from the surface, we observe (Fig. 2) as did Nishi *et al.*,[24] desorbed H_2 molecules. Even thermalized H atoms were seen[22] to be desorbed from ammonia films by 193 nm radiation. Hydrogen loss limits back reactions and enhances the production of NH_2 and N_2.

B. Ammonia destruction studied via infrared spectroscopy

To quantify the destruction of pure ammonia and ammonia in the ammonia–water mixture as a function of fluence, we calculated the band areas of absorption features at both 4523 and 1100 cm^{-1} and normalized each initial band area to unity so that we could compare trends (Fig. 6). We note that the analysis is complicated at low fluences ($<1 \times 10^{19}$ photons/cm^2) by band sharpening and at high fluences (above 10^{19} photons/cm^2) by photodesorption. Figure 6 (top) shows that for pure ammonia, the initial trends are different, depending on which band we use, even though their final value is similar (0.73 versus 0.78), which may be explained by the band sharpening.

This situation is more simplified in the experiments where ammonia is in the water mixture, since photolysis induces no significant changes in the band shapes and very little photodesorption. However, as can be seen in Fig. 6, analysis of each band still yields different results: the 4523 cm^{-1} band increases slightly in the beginning and then subsequently decreases for a net loss of $\sim$5%, while the band at 1100 cm^{-1} decreases from the beginning by about 20%. Moreover, by fitting the Fresnel equations to our UV reflectance spectra,[23,29] we find that the density of our sample increases from 0.84 to 0.91 g/cm^3 during photolysis. Thus, we suspect that this difference in each bands behavior is likely an optical
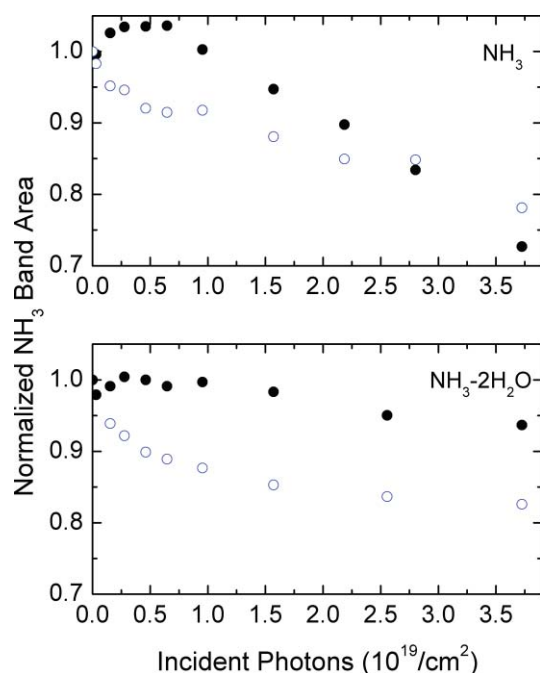
FIG. 6. Normalized NH_3 band area in both the pure NH_3 and $NH_3 \cdot 2H_2O$ samples as a function of fluence, calculated from the 4523 cm^{-1} (●) and 1100 cm^{-1} (○) ammonia absorption bands. We note that for both samples, each band yields a different behavior (see text).

FIG. 7. Theoretical reflectance curves for a 1:2 NH_3–H_2O mixture grown at 40 K with a density of 0.84 g/cm^3 (solid) and 0.91 g/cm^3 (dashed). Curves were derived from optical constants obtained from our unirradiated sample (0.84 g/cm^3).

interference effect induced by the thickness reduction of the sample. To verify this, we obtained optical constants for our initial spectrum (see Ref. 30 for procedure) and then used those optical constants to produce a theoretical reflectance spectrum of our ammonia–water mixture with the increased density of 0.91 g/cm^3 (Fig. 7). As can be seen in Fig. 7, this density increase (compaction) affects the apparent absorption band strength at 1100 cm^{-1} band but not the 4523 cm^{-1} band (Fig. 7). The fact that one band is effected more than another is a common consequence of optical interference effects, since they depend on wavelength. Similar to the decrease at 1100 cm^{-1}, the water absorption feature at 850 cm^{-1} also decreases during irradiation (Fig. 7), even though there is no indication of water decomposition. Thus, infrared spectroscopy verifies that while there is some decomposition of ammonia, the amount destroyed is at least a factor of three less than the amount sputtered for a sample of pure ammonia, indicating that the water matrix may actually inhibit the destruction and removal of ammonia.

This effect is opposite to what is found with ion irradiation, where water enhances decomposition of ammonia mixtures,[3] which can be explained by radiolytic OH destroying ammonia by forming nitrogen oxides, such as NO and N$_2$O, as recently reported in irradiated ammonia–water ices.[18] The fact that the photons used in this work cannot produce OH, can explain the absence of enhanced ammonia destruction but, by itself, not the opposite effect, a decreased probability of dissociation. We propose that the explanation resides in the shift of the near-edge absorption spectrum of ammonia due to the presence of water. In pure ammonia, the 6.4 eV photons can excite with high probability an excitonic state, the solid state analog of a Rydberg state of a nitrogen lone-pair electron in the gas phase.[31] The exciton energy is
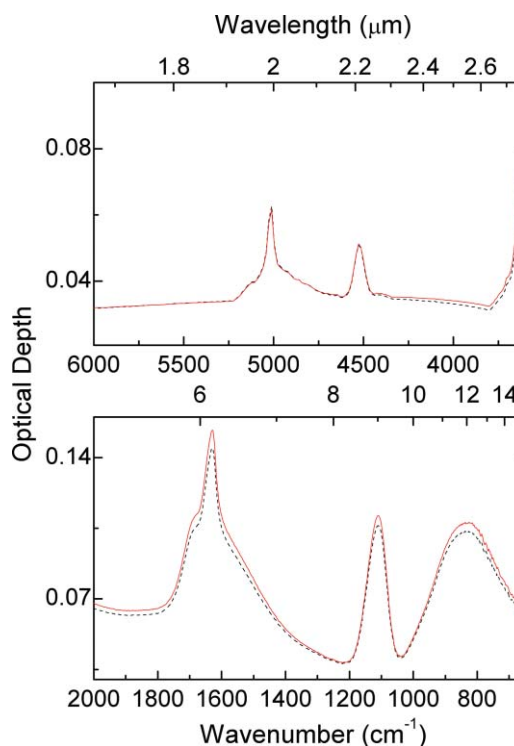
shifted due to dielectric screening in the solid and due to repulsive interactions with nearby molecules. As a result the energy, and also the width, of the exciton depends strongly on the local environment.[20] In particular, the addition of a bonding water molecule displaces the absorption edge of ammonia to higher energies.[32] The net effect is a much reduced photoabsorption cross section in the hydrate, explaining why the water matrix inhibits the destruction and removal of ammonia.

We now calculate the quantum yield for photodestruction (dissociation plus desorption) of our pure ammonia sample. A fluence of 3.7×10^{19} photons/cm^2 destroys/photodesorbs ∼25% of NH$_3$, determined using the average of the attenuation of the 4523 cm^{-1} and 1100 cm^{-1} band. Using a photoabsorption cross section of 1.3×10^{-18} cm^2 at 40 K, interpolated from measurements by Dawes *et al.* at 25 and 75 K, and considering a 20% probability of reflection for photons reaching the gold substrate, we estimate that only 62% of the incident flux is absorbed by the film. Hence, the quantum yield is extremely low ∼0.01, or ∼99% of the 6.4 eV energy of each absorbed photon is dissipated as heat without dissociation. This observation supports the view, given above, that the sharpening of absorption features with fluence is due to local heating around the absorbing molecule.

C. Photodesorption

Nishi *et al.* (1984) found that the energy distribution of photodesorbed NH$_3$ can be described by two Maxwell–Boltzmann distributions, with mean translational energies of

0.17 eV (low) and 0.65 eV (high), which can be compared with 0.25 eV, the surface binding energy of solid ammonia.[33] The low energy component has a peak energy of 0.11 eV, which being about one half of the binding energy, can be associated with molecules ejected from a cascade of collisions in the solid initiated by an absorbed photon, similar to the case of sputtering.[34] The high-energy component, comprising 0.545 of the total, is most likely to be associated with excited surface molecules that lose very little energy on desorption.

Since the total desorption yield we measured is 0.0011, the yield of the hot or surface component of NH_3 desorption is 0.0006. On the other hand, the probability that one of the $\sim10^{15}/cm^2$ surface molecules absorbs a 193 nm photon is 0.0013 since the photoabsorption cross section is 1.3×10^{-18} cm^2. If the excitation is localized at the surface, then there is a probability of $0.0006/0.0013 = 0.46$ of photodesorption by a surface excitation.

We note that while gas phase photoabsorption gives rise to a Rydberg state followed by fragmentation (NH_2 + H), absorption in the solid state forms an exciton. Thus, rather than dissociation, the repulsion of the extended exciton with neighboring molecules causes desorption. This is the "electron exchange repulsion" mechanism discussed by Nishi *et al.*,[21] very similar to the "cavity ejection" mechanism in the rare-gas solids due to self-trapped excitons.[35] If the exciton is able to diffuse and trap at a low energy surface site, then photons absorbed in the bulk will be able to contribute to the hot surface component of desorption.

Desorption by cavity ejection may also occur in ammonia–water mixtures, but the nature of the exciton will change, which will radically decrease the probability of photoabsorption. An alternative explanation was proposed[21] on the assumption that NH_3 molecules clustered into islands in the H_2O matrix. However, the NH_3–H_2O equilibrium phase diagram[5] shows that, at the temperature of the experiments by Nishi *et al.*[21] (90–130 K) the ammonia molecule is most likely mixed in water and not in clusters.

D. Absorption at ~1508 cm^{-1}

This weak absorption band is important in connection to the "6.85 μm absorption" (1437–1473 cm^{-1}) seen in interstellar clouds toward embedded young stars, as discussed by Schutte & Khanna.[36] These authors photolyzed mixed ices of ammonia and H_2O, CO_2, and O_2 with hard UV photons that included Lyman-α (10.2 eV) and formed an absorption band that peaked at ~1480 cm^{-1} and shifted to 1420 cm^{-1} during warming. They assumed that the absorption is due to NH_4^+ ions, balanced in charge by unidentified negative counter ions that do not display distinctive absorptions. This assignment is based on experiments[37] that showed ammonia embedded in solid Ne and irradiated with broad UV light produces an absorption at 1447 cm^{-1}. In an experiment designed to test the NH_4^+ interpretation, Maté *et al.*[38] showed that frozen aqueous solutions of $NH_4^+Cl^-$ produced a muted band at ~1400 cm^{-1}, and thus concluded that if the "6.85 μm absorption" is indeed due to NH_4^+, then the ice must contain other species that can alter the band position and intensity significantly.

Numerous radiation chemical studies of pure NH_3 or NH_3 mixed in water have produced an absorption band at ~1500 cm^{-1}, which has also typically been attributed to NH_4^+. Reported values, in cm^{-1}, are 1505 in photolyzed NH_3 (Ref. 19), 1506–1505 cm^{-1} in ion irradiated NH_3:H_2O (Refs. 3 and 18), 1514 in electron irradiated NH_3 (Ref. 39), 1515 cm^{-1} in photolyzed NH_3:H_2O (Ref. 40) and the values of 1507 and 1496 cm^{-1} measured in this work for NH_3 and NH_3:H_2O ices. Based on the recent results that show NH_4^+ appears at ~1400 cm^{-1} in ice[38] and from the fact that the 6.4 eV photons in our experiments have insufficient energy to produce ionization in pure NH_3 or the hydrate, or produce a lower energy ion pair such as $NH_4^+ - NH_2^-$, we do not assign the ~1500 feature to NH_4^+. Among the neutral species, an obvious candidate is NH_2, which is a well known photodissociation product and which has an absorption band at 1499 cm^{-1}.[37]

E. Astronomical implications

Ammonia in astronomical environments is unlikely to be in pure form but rather mixed in hydrates, which are lower energy forms in thermodynamic equilibrium. Our results, together with photoabsorption cross sections,[20] show that the hydrate will be more resistant to solar radiation than pure ammonia between the threshold at ~205 and ~190 nm. Photons of shorter wavelength are unlikely to be important in ammonia hydrate destruction, because the solar flux decreases very rapidly with wavelength in this region and the absorption by water increases dramatically below ~150 nm, such that the photons penetrate less than ~100 nm below the surface. The shallow penetration depth for these photons, including the intense photon flux near Lyman-α, is orders of magnitude smaller than the depth sampled by near-IR remote sensing, implying that the low abundances detected by near-IR remote sensing cannot be explained by photolysis alone but may be due to an intrinsic low ammonia concentration in the bulk of the ice. Ammonia close to the surface can also be destroyed by other processes such as energetic electron or ion irradiation.[3,16–18] Furthermore, micrometeorite impact may also contribute to ammonia depletion, as they will cause localized heating and garden the surface. Localized heating will bring fresh ammonia to the surface, where it can be removed by radiation processes, or it may simply preferentially sublimate ammonia, since it is more volatile than water ice. Gardening will mix the surface and subsurface material, which over time will increase the thickness of the depleted layer.

V. CONCLUSIONS

In this study, we have shown the destruction of ammonia and relative stability of the ammonia-dihydrate under photolysis with a 193 nm laser at 40 K. For the pure NH_3 sample, besides NH_3, we observe the ejection of H_2 and N_2 increasing with fluence, indicating a buildup of these new species in the ice. This behavior of the N_2 ejection explains the increase in mass loss rate with fluence observed with the microbalance. For the ammonia–water mixture, we see a very weak signal of H_2 and N_2 in the mass spectrometer, consistent with the microbalance results that show essentially no mass loss

during the experiment. After accounting for the changes in optical properties induced by the compaction of the ice film, we determine that the destruction of the ammonia in the ammonia–water sample is <5%, as explained by a lower photoabsorption cross section caused by a blue-shift in the photoabsorption threshold.

ACKNOWLEDGMENTS

[1] J. S. Kargel, Icarus **100**, 556 (1992).

[2] J. S. Holt, D. Sadoskas, and C. J. Pursell, J. Chem. Phys. **120**, 7153 (2004); J. E. Bertie and M. R. Shehata, *ibid.* **83**, 1449 (1985); *ibid.* **81**, 27 (1984).

[3] M. H. Moore, R. F. Ferrante, R. L. Hudson, and J. N. Stone, Icarus **190**, 260 (2007).

[4] H. Kawakita and J.-I. Watanabe, Astrophys. J. **572**, L177 (2002).

[5] D. L. Hogenboom, J. S. Kargel, G. J. Consolmagno, T. C. Holden, L. Lee, and M. Buyyounouski, Icarus **128**, 171 (1997).

[6] J. S. Lewis, Icarus **16**, 241 (1972); D. J. Stevenson, Nature **298**, 142 (1982).

[7] J. S. Kargel, Earth, Moon, Planets **67**, 101 (1994).

[8] C. C. Porco, P. Helfenstein, P. C. Thomas, A. P. Ingersoll, J. Wisdom, R. West, G. Neukum, T. Denk, R. Wagner, T. Roatsch, S. Kieffer, E. Turtle, A. McEwen, T. V. Johnson, J. Rathbun, J. Veverka, D. Wilson, J. Perry, J. Spitale, A. Brahic, J. A. Burns, A. D. DelGenio, L. Dones, C. D. Murray, and S. Squyres, Science **311**, 1393 (2006).

[9] J. S. Kargel and S. Pozio, Icarus **119**, 385 (1996).

[10] S. J. Ostro, R. D. West, M. A. Janssen, R. D. Lorenz, H. A. Zebker, G. J. Black, J. I. Lunine, L. C. Wye, R. M. Lopes, S. D. Wall, C. Elachi, L. Roth, S. Hensley, K. Kelleher, G. A. Hamilton, Y. Gim, Y. Z. Anderson, R. A. Boehmer, W. T. K. Johnson, and the Cassini RADAR Team, Icarus **183**, 479 (2006).

[11] D. R. Stegman, J. Freeman, and D. A. May, Icarus **202**, 669 (2009).

[12] J. H. Waite, Jr., W. S. Lewis, B. A. Magee, J. I. Lunine, W. B. McKinnon, C. R. Glein, O. Mousis, D. T. Young, T. Brockwell, J. Westlake, M.-J. Nguyen, B. D. Teolis, H. B. Niemann, R. L. McNutt, Jr., M. Perry, and W.-H. Ip, Nature **460**, 487 (2009).

[13] M. E. Brown and W. M. Calvin, Science **287**, 107 (2000); C. Dumas, R. J. Terrile, R. H. Brown, G. Schneider, and B. A. Smith, Astron. J. **121**, 1163 (2001).

[14] J. P. Emery, D. M. Burr, D. P. Cruikshank, R. H. Brown, and J. B. Dalton, Astron. Astrophys. **435**, 353 (2005); A. J. Verbiscer, D. E. Peterson, M. F. Skrutskie, M. Cushing, P. Helfenstein, M. J. Nelson, J. D. Smith, and J. C. Wilson, Icarus **182**, 211 (2006).

[15] L. J. Lanzerotti, W. L. Brown, K. J. Marcantonio, and R. E. Johnson, Nature **312**, 139 (1984).

[16] M. J. Loeffler, U. Raut, and R. A. Baragiola, Astrophys. J. **649**, L133 (2006).

[17] G. Strazzulla and M. E. Palumbo, Planet. Space Sci. **46**, 1339 (1998).

[18] M. J. Loeffler, U. Raut, and R. A. Baragiola, J. Chem. Phys. **132**, 054508 (2010).

[19] P. A. Gerakines, W. A. Schutte, and P. Ehrenfreund, Astron. Astrophys. **312**, 289 (1996).

[20] A. Dawes, R. J. Mukerji, M. P. Davis, P. D. Holtom, S. M. Webb, B. Sivaraman, S. V. Hoffmann, D. A. Shaw, and N. J. Mason, J. Chem. Phys. **126**, 244711 (2007).

[21] N. Nishi, H. Shinohara, and T. Okuyama, J. Chem. Phys. **80**, 3898 (1984).

[22] E. Lanzendorf, D. P. Masson, and A. C. Kummel, J. Chem. Phys. **103**, 7585 (1995).

[23] M. J. Loeffler, B. D. Teolis, and R. A. Baragiola, J. Chem. Phys. **124**, 104702 (2006).

[24] N. J. Sack and R. A. Baragiola, Phys. Rev. B. **48**, 9973 (1993).

[25] A. D. Fortes and M. Choukroun, Space Sci. Rev. **153**, 185 (2010).

[26] L. R. Canfield, G. Hass, and W. R. Hunter, J. Phys. **25**, 124 (1964).

[27] O. Ellegaard and J. Schou, J. Appl. Phys. **83**, 1078 (1998).

[28] S. Leach, H.-W. Jochims, and H. Baumgartel, Phys. Chem. Chem. Phys. **7**, 900 (2005); M. Suto and L. C. Lee, J. Chem. Phys. **78**, 4515 (1983).

[29] M. S. Westley, G. A. Baratta, and R. A. Baragiola, J. Chem. Phys. **108**, 3321 (1998).

[30] B. D. Teolis, M. J. Loeffler, U. Raut, M. Famá, and R. A. Baragiola, Icarus **190**, 274 (2007).

[31] M. B. Robin, *Higher Excited States of Polyatomic Molecules* (Academic, London, 1974).

[32] J. R. Lane, V. Vaida, and H. G. Kjaergaard, J. Chem. Phys. **128**, 034302 (2008).

[33] A. S. Bolina and W. A. Brown, Surf. Sci. **598**, 45 (2005).

[34] P. Sigmund, Phys. Rev. **184**, 383 (1969).

[35] F. Coletti, J. M. Debever, and G. Zimmerer, J. Phys. Lett. **45**, 467 (1984); G. Zimmerer, Nucl. Instrum. Methods Phys. Res. B **91**, 601 (1994).

[36] W. A. Schutte and R. K. Khanna, Astron. Astrophys. **398**, 1049 (2003).

[37] D. E. Milligan and M. E. Jacox, J. Chem. Phys. **43**, 4487 (1965).

[38] B. Maté, O. Gálvez, V. J. Herrero, D. Fernández-Torre, M. A. Moreno, and R. Escribano, Astrophys. J. **703**, L178 (2009).

[39] W. Zheng, D. Jewitt, Y. Osamura, and R. I. Kaiser, Astrophys. J. **674**, 1242 (2008).

[40] E.-S. Moon, H. Kang, Y. Oba, N. Watanabe, and A. Kouchi, Astrophys. J. **713**, 906 (2010).